International Journal of Power Electronics and Drive System (IJPEDS)
Vol. 17, No. 1, March 2026, pp. 95~106
ISSN: 2088-8694, DOI: 10.11591/ijpeds.v17.i1.pp95-106

Linearity analysis of a brushed DC machine thermal system in response to speed input using transfer function

M. S. Mat Jahak, M. A. H. Rasid
Faculty of Manufacturing and Mechatronics Engineering Technology, Universiti Malaysia Pahang Al-Sultan Abdullah, Pekan, Malaysia

Article Info

Article history:

Received Jul 23, 2024
Revised Nov 25, 2025
Accepted Dec 11, 2025

Keywords:

Electrical machines
Reduced-model
Thermal analysis
Thermal model
Transfer function

ABSTRACT

This study represents a preliminary step toward developing a real-time condition monitoring system for brushed DC machines by analyzing the linearity of their thermal behavior. The temperature response of an MY1016 DC motor was collected under no-load conditions at five different speed levels, ranging from 20% to 100% of the rated speed, until the motor reached steady-state conditions to emphasize the temperature increase due to speed variability. A transfer function model was identified using MATLAB's System Identification Toolbox, and the system's linearity was evaluated by analyzing the spread of pole values across different speeds. Results showed significant variability in the coefficient of variation (CV) for key components, with values ranging from 0.18 for the casing to 0.84 for the brush. These findings reveal significant deviations from linear thermal behavior, indicating that a single linear transfer function may be insufficient to model the system. This research highlights the need to validate linearity assumptions in thermal modeling and introduces a framework for assessing thermal variability under varying speed conditions.

Corresponding Author:

M. A. H. Rasid
Faculty of Manufacturing and Mechatronics Engineering Technology
Universiti Malaysia Pahang Al-Sultan Abdullah
26600 Pekan, Pahang, Malaysia
Email: mahizami@umpsa.edu.my

1. INTRODUCTION

Motors account for 40% of global electricity consumption and 13% of carbon emissions, and often suffer irreversible thermal damage [1]. To reduce the risk of irreversible damage, an anomaly detection system can help alert the user to any potential faults in the machine. Scheduled periodic visual inspections and recording this data are valuable information when reviewing the machine's performance. The simplest way to monitor the machine's health is to regularly inspect and provide a written report as proposed in [2]. These written inspection reports perform much better than the memory of the maintenance technician or supervisor when questioning the performance history of a certain piece of equipment. It proposes a generic inspection guideline for motor health records. However, this is costly and time-consuming. Therefore, online condition monitoring of electric motors has gained importance over the past 30 years due to reducing machine downtime in critical applications and enhancing their reliability [3].

Among the most frequent faults occurring in brushed electrical machines are overload, a lack of lubrication, repeated motor starts/stops, and insufficient cooling. Under these conditions, electric motors are exposed to undesirable stresses, which put the motors at risk of faults or failures [4]-[6]. According to IEEE Recommended Practice for the Design of Reliable Industrial and Commercial Power Systems in 2007 (refer Table 1), motor components that suffer from faults in order are bearing (41%), stator (37%), rotor (10%), and

other (12%) [7]. Besides that, according to selected articles from 2006-2018, the most common faults and their statistical incidences are listed in Table 2. These statistical analyses provide valuable insights into common fault types. Furthermore, they highlight the critical needs for monitoring and predictive tools for thermal behavior in motors, which could serve as early indicators of potential failures. Addressing this gap, the present study will focus on thermal response variability in motor components, providing a novel framework for real-time condition monitoring and fault detection.

Table 1. A pole statistical study by IEEE recommended practice for the design of reliable industrial and commercial power systems in 2007

	Number of faults				
Type of fault	Induction motors	Synchronous motors	Wound rotor motors	DC motors	All motor types (total)
Bearing	152	2	10	2	166
Winding	75	16	6	-	97
Rotor	8	1	4	-	13
Shaft	19	-	-	-	19
Brushes or slip rings	-	6	8	2	16
External devices	40	7	1	-	18
Others	10	9	-	2	21

Table 2. Statistics of common faults according to recent research

	Number of faults				
Type of fault	Induction motor	Synchronous motor	Wound rotor motor	DC motor	All motor types (total)
Bearing	21	-	-	3	24
Winding	22	3	1	3	28
Rotor	34	2	-	-	36
Shaft	3	-	-	-	3
Brushes	-	-	-	2	1
External devices	5	1	-	2	8
Air gap eccentricity	14	3	1	-	18
Others	9	3	-	3	14

Among the monitoring methods used, the most frequently used methods for monitoring motor health are the motor current signal analysis (MCSA) [8]-[10] and vibration analysis [11]-[14]. However, they are costly and need highly trained analysts. A more recent integration of machine learning methods has also gained interest among diagnosticians [15]-[17]; however, collecting sufficient historical data to train machine learning models remains expensive in terms of instrumentation and time-consuming. To reduce the cost of health monitoring, another method can be potentially used: thermal behavior assessment of the machine [18], [19]. To build a proper temperature monitoring system for the components of the motor, the classic solution is to equip the motor with temperature measurement instrumentation. However, this leads to additional costs and cable management issues. It could be too much for a system equipped with many motors [20], [21]. The less instrumented option is to have a real-time model that estimates the temperature of the components inside the motor using a single input, like the speed or current of the motor [22]. All these three methods have their merits and advantages as well as inconveniences.

Several studies have used transfer functions as thermal models for electric machines for high accuracy, low computational resources [23], and easy implementation [24], [25] have established thermal error compensation using a transfer function to model the relationship between heat sources and the resulting thermal errors in machine tools, which can affect machining accuracy. Additionally, [26] presents online thermal monitoring of induction machines using a transfer function, focusing on accurately calculating both average and hotspot temperatures [27]. Simplified the first-order transfer function to model the stator winding temperature using only three parameters as in (1). The parameters considered were T_s temperature rise, k_1 and k_2 are $Loss_1$ and $Loss_2$ which were considered constant and independent of any load change after a certain amount of operating time, τ_1 is the time constant and I_s^2 is the current drawn by the motor. The response of the first-order transfer function is illustrated in Figure 1.

$$T_s(t) = k_1 I_s^2 \left(1 - e^{-\frac{t}{\tau_1}}\right) + k_2 \quad (1)$$

In our project, a real-time model using a transfer function will be developed. The transfer function in a single node should be able to precisely estimate the baseline temperature of a brushed DC machine operated at different speeds. To achieve such a transfer function, it needs to be verified whether the thermal

response of a DC machine is linear-time invariant (LTI) or not. An LTI system would mean that the transfer function of the system is constant for all speeds. With potential small and negligible discrepancies, different speeds may need different transfer functions. Nevertheless, they should be close to where the pole values should be observed to have a very small variation in terms of their values. So, in this study, the transfer function that models the thermal response of a brushed DC machine is analyzed to verify the system linearity. The novelty of this study lies in developing a simplified yet accurate thermal model for brushed DC motors through transfer function analysis, and in evaluating system linearity across speeds. This approach has not been explored in the current literature to our knowledge, particularly regarding non-linear behavior in thermal responses. The process of this evaluation is explained in the next section of the methodology.

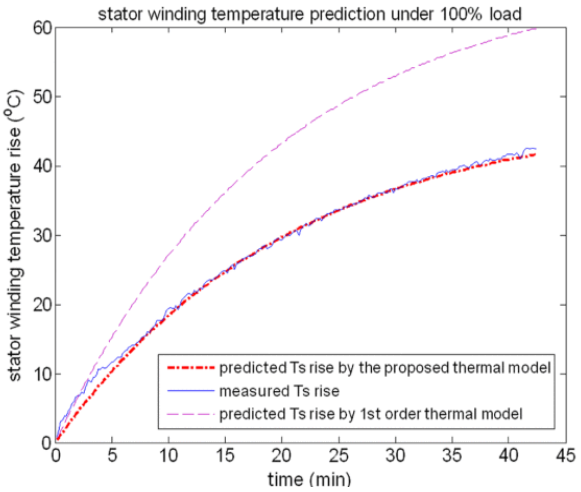

Figure 1. Temperature estimation under 100% load condition [27]

2. METHOD

The research starts with temperature response data collection using an experimental setup, which will be used as input to develop our model. The next step is the identification of transfer function models that can model precisely the temperature responses at different speeds. Finally, the transfer function deduced will be analyzed by observing its pole positions on an s-plane and identifying the spread between these poles by computing the standard deviation and coefficient of variation, CV. A small spread will signify a system that is close to being LTI, while the opposite observation would mean that the system is not LTI. A non-LTI system cannot, therefore, be presented using a single transfer function to present the thermal response across a different speed range. The following subsections explain in detail each step.

2.1. Temperature response data collection

The temperature response of MY1016 DC machines was collected with the motor operated using a programmed block diagram in Simulink for speed control and data acquisition. The DC motor was run in a continuous cycle at no load until it reached temperature equilibrium, as specified in the IEC-60034 standard for motor testing for the cycle S1. It was run at no load to focus on the influence of speed-dependent temperature increases, which are primarily caused by frictional contact at the brush and commutator interface. Under loaded conditions, the dominant contributor to temperature rise is the copper losses, which are linearly dependent on the motor current [28]. This load-dependent increase can overshadow the speed-dependent effects, making them less distinguishable. The no-load condition, therefore, provides a clearer insight into the thermal behavior driven by speed variations, particularly for small motors where frictional losses play a significant role.

This process was repeated at different motor speeds, starting at 20% and increasing in increments of 20% up to 100%. These speeds were calculated relative to the rated speed of the MY1016, which is 2650 rpm. Thermocouples were used to measure the temperature response at various parts of the DC machines, including the brush, bearing, permanent magnet, and casing, as visualized in Figure 2(a). The thermocouples are placed at the location of the hotspot of each component following previous observations using thermal imaging [18]. This is a necessary step to ensure that the temperature used in the transfer function identification will not underestimate the temperature of the components at any location. The temperature of the motor must achieve a steady state before ending the duty cycle. If the temperature continues to rise and

change, the process of data acquisition continues until it reaches a steady state. Once all the data has been collected, it is plotted and analyzed. The complete experiment setup can be seen in Figure 2(b). This data was then used to identify the transfer function of the temperature response.

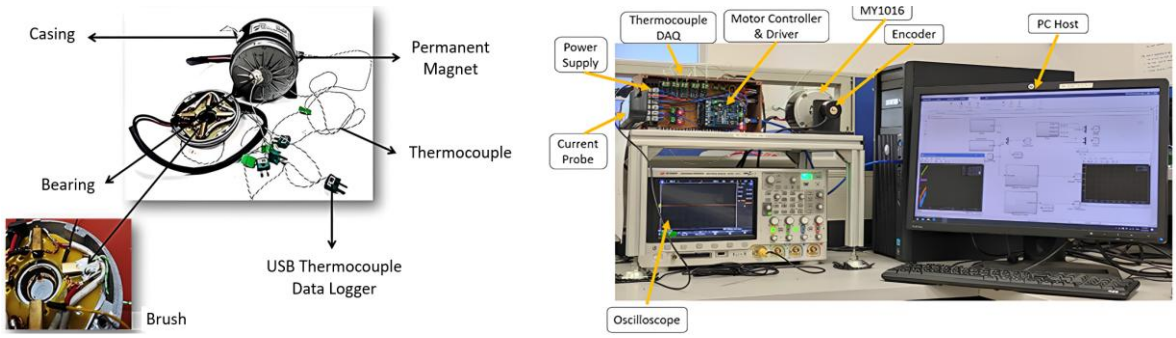

Figure 2. The temperature data collection setup: (a) instrumentation of DC machines with thermocouples and (b) the complete test setup

2.2. Experimental setup

The outputs from the thermocouples are monitored using a type-K thermocouple unit with an error of +/- 1.1 ℃. The thermocouple measurements are taken automatically every 0.25 seconds, and the data is transmitted to a host PC for storage. The current is monitored using the TP-CC80 current clamp, which allows the oscilloscope to measure electrical currents up to 80 A ac/dc, with a frequency response of up to 20 kHz. The speed is measured using a rotary encoder with 500 pulses per revolution, which is programmed to be monitored along with the temperature. Once the DC motor is completely instrumented, the motor is mounted on the top of the test bench.

The motor studied is a small, brushed DC motor, commonly named MY1016. This choice was made due to the ease of disassembly and installation of the machine, as well as the accessibility to implement thermocouples on components such as the brush, bearing, permanent magnet, and casing. In addition, the structure of the machine is quite complex with irregular surfaces and cavities in the airgap, leading to unpredictable temperature behavior, which is interesting to observe. This complexity arises from the intricate components, the closed and rough surface on the inside, and the turbulent effect of air circulation. The specifications of the DC motor can be found in Table 3. This motor can be commonly found in small actuator applications for light mobility, such as electric bicycles and scooters. Small-scale semi-industrial applications such as conveyors, extruders, fans, and ventilators for food processing, and agro-industrial machinery are also frequent users of this inexpensive motor.

Table 3. Specification of the MY1016 brushed DC machines

Parameters	Values
Model	MY1016
Operating voltage	24 VDC
Rated current	13.5 A
Rated speed	2650 Rpm
Operating power/output	250 W
Rated torque	100 N-cm
No load current	<2.2 A
Shaft diameter	12.2 mm
Cable length	25 cm
Weight	2.0 Kg
Dimension	(20×15×10) cm

2.3. Transfer function identification using system identification toolbox

The system identification toolbox of MATLAB is here deployed. The temperature response data was set as the output response, while the PWM step speed input value was set as input and imported to the system identification Import Data section, as shown in Figure 3(a). The toolbox enables us to find the corresponding transfer function of the imported temperature response. By selecting the transfer function as

the model of choice, two parameters need to be set, which the toolbox will try to find and fit to the experimental data. Transfer functions' parameters needed are the number of zeros and poles of the transfer function. Their chosen values need to be set in the toolbox as shown in Figure 3(b). The generic form of a transfer function, considering its poles, is shown in (2) with n the order of the system, a a real number, and the values of s solving the polynomials in the denominator are the poles.

$$G(s) = \frac{1}{a_n s^n + a_{(n-1)} s^{(n-1)} + \ldots + a_0} \quad (2)$$

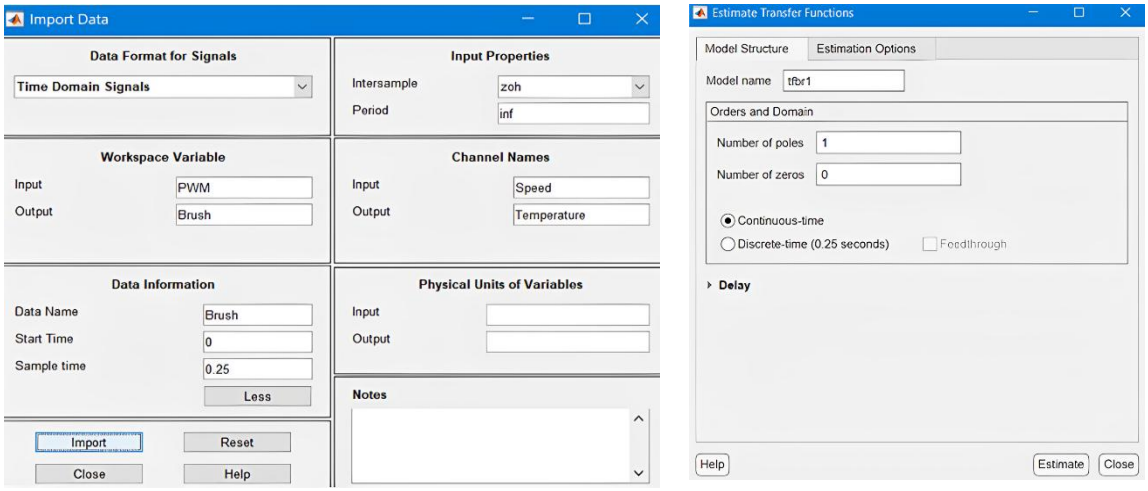

(a) (b)

Figure 3. The interface for input temperature data import: (a) import data step input and temperature response to the system identification toolbox and (b) setting the pole and zeros parameter

No zeros were chosen for the transfer function, as a physical system can usually be modelled with no zeroes. Only gain will take place on the numerator. For the poles, different values were tested, ranging from a single pole to four poles, representing systems of the first to fourth order. The reason for limiting the pole value to 4 is that choosing a high pole value can lead to an unstable system. The requirement that all poles need to be in the left half of the complex plane, as mentioned by [29] and [30] (chapter basic control system and effects adding poles and zeros to transfer functions), will become too constraining. Higher-order models tend to overfit the experimental data, capturing noise or minor variations that do not represent the underlying system dynamics. This overfitting increases the prediction error when the model is applied to new data. Transfer functions with more than four poles may also exhibit instability, with poles appearing in the right-half s-plane, violating the requirement for a physically stable system.

In most cases, thermal responses are best approximated by low-order models due to the absence of oscillatory behavior typically associated with higher-order systems. A temperature response resembles a first-order response. It could not be physically considered a second-order system, as there is no possibility of temperature oscillations like in mechanical or electrical systems. However, the purpose of considering higher orders (2 to 4) is to evaluate the possibility of having a higher precision model, which is purely a mathematical model and not necessarily attached to a physical reality. Physically, it could be considered a higher-order system with a high damping value (an overdamped system). This is particularly useful for a model that is going to be used solely to monitor the baseline temperature with high precision, without considering its potential use in optimization model purposes.

Figure 4(a) illustrates the estimated transfer function result in system identification for all components with the choices of pole number. The same Figure 4(b) also shows the prompt that gives the model estimation error. The estimation of the transfer function was done without preprocessing and splitting experimental data. This practice has been employed by several researchers [31]-[33] for the estimation of transfer function using system identification. It is justified by the low mean squared error (MSE) result. The choice of lower order (up to 4) is also less sensitive to overfitting to the extremely dynamic noises in temperature measurements observed.

The table on the right of Figure 4(a) shows the model estimation using the transfer function that the toolbox found for different motor components. By row: brush, bearing, permanent magnet, and casing, and by column: 1st order, 2nd order, 3rd order, and 4th order. It also provides the equation of the transfer function in

the form of polynomials as presented in (2). These outputs are generated for one of the speed points that was tested. The identification process is repeated for all the speed points tested from 20% to 100% of the nominal speed of the motor. These model outputs will be later presented in the result chapter. To select the best model between the order choices, the error of the model evaluated will be assessed, which will also be presented in the next section.

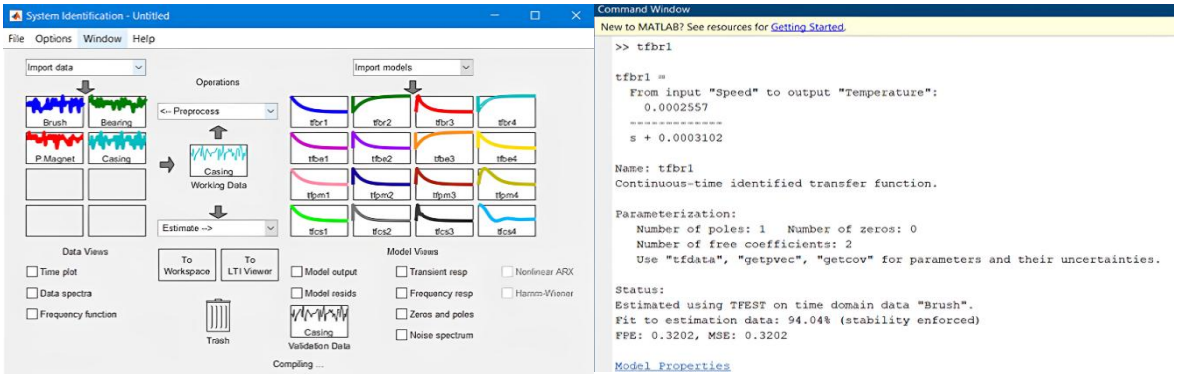

(a) (b)

Figure 4. Output of system identification toolbox: (a) result estimation transfer function in system identification and (b) error of estimation prompt

2.4. System linearity analysis

From the transfer functions generated by the system identification, the pole values are extracted by acknowledging that any transfer function written in polynomial form of $G_{k\,N}(s) = \frac{Z_{k\,N}(s)}{\sigma_{k\,N}(s)}$ can be decomposed as shown in (3).

$$G_{k\,N}(s) = \frac{Z_{k\,N}(s)}{\sigma_{k\,N}(s)} = K_{k\,N}\frac{(s-Z_{1k\,N})(s-Z_{2k\,N})\ldots(s-Z_{1k\,N})}{(s-\sigma_{1k\,N})(s-\sigma_{2k\,N})\ldots(s-\sigma_{3k\,N})} \quad (3)$$

Where $Z_{k\,N}(s)$ is the zero function for the component k at speed N, $\sigma_{k\,N}(s)$ is the pole function for the component k at speed N, $K_{k\,N}$ is the gain, $Z_{1k\,N}$ to $Z_{3k\,N}$ the zero values, and $\sigma_{1k\,N}$ to $\sigma_{3k\,N}$ are the pole values. The number of poles depends, of course, on the order of the transfer function chosen.

The poles extracted are then plotted on the s-plane to be observed. Figure 5 shows a *pzplot* example for the component brush, a component where the error of the model estimation indicates that the 3rd order is the best order to represent its temperature response. Notice that the brush has three poles represented as "X" for every nominal speed. The poles of the brush are color-coded to represent their nominal speed. Red indicates 20%, blue indicates 40%, green indicates 60%, yellow indicates 80%, and purple indicates 100% of the nominal speed. The pole on the x-axis is a real pole, while the y-axis represents a complex conjugate pair of poles. All the brush poles on the complex s-plane are in the left-half plane, which means they are in the stable region. Also, a typical third-order transfer function may have one real pole and a complex conjugate pole pair, which is the necessary and sufficient condition to have real-valued coefficients in the differential equation representing the system. There are no zeros represented as "O" in the s-plane graph because, as mentioned before, the identified transfer function was chosen to have no zeros for all components, including the brush, bearing, permanent magnet, and casing.

Once the values of the poles are found, the variance values between the poles are deduced. It is calculated by finding the squared difference of each data point from the mean and then dividing it by the number of data points. It is used to compare the spread or dispersion of different data, in this case, the pole values. To calculate it, the mean value, $\overline{\sigma_k}$ is first calculated by (4), then the variance, S^2 using in (5). The coefficient of variation, CV, which compares the standard deviation to the mean value of the pole, is also then calculated to assess how far the spread is from the mean value of the pole using (6) with $\sigma_{k\,N}$ is the transfer function of the component k at speed N, N_{min} to N_{max} are the minimum to the maximum speed at which the transfer functions were identified, and n_N the number of speeds tested.

$$\overline{\sigma_k} = \frac{\sum_{N_{min}}^{N_{max}} \sigma_{k\,N}}{n_N} \quad (4)$$

$$S^2 = \frac{\sum_{N_{min}}^{N_{max}} (\sigma_{k\,N} - \overline{\sigma_k})}{n_N} \quad (5)$$

$$CV = \sqrt{S^2} \Big/ \overline{\sigma_k} \quad (6)$$

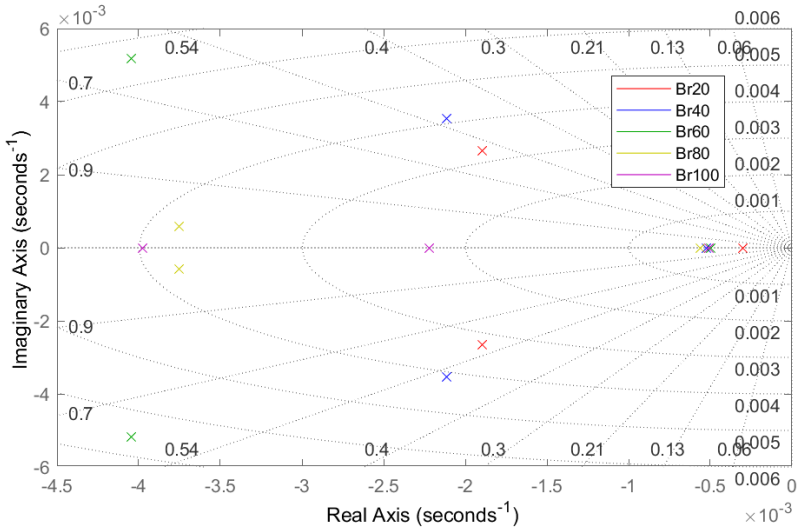

Figure 5. S-plane graph of pole brush

3. RESULTS

In this section, the result will be presented in two parts. The first one will present the identified transfer functions and discuss the choice of order chosen for each component. Then, the second part will present the linearity analysis of the transfer functions of each component as the motor speed changes.

3.1. Identified transfer function

Following the identification process using the identification toolbox, the best order to represent the temperature response of each motor's component is to be chosen. Tables 4 to 7 below show the transfer function obtained and the estimation error for each choice of pole number at different speeds tested for the brush. The best model is chosen by selecting the model with the lowest MSE error across all speeds. Interestingly, the 1-pole model and 3-pole model consistently have the lowest MSE error for all speed ranges. To choose between these two pole numbers, an observation at the speed of 60% shows that the 3-pole model has a lower maximum MSE error than the 1-pole model, respectively at 0.41 and 0.65. This shows the pole 3-pole model is a better order for the identified transfer function model, and thus is selected to represent the temperature response of the component brush. The 2-pole and 4-pole models are too far from being precise, with a huge MSE error observed. As for other components other than the brush, a first-order transfer function was found to be the most precise. The values of the poles of the chosen transfer function will be presented in the next section for all components for a linearity analysis.

Table 4. 1-pole transfer function model

Pole no.	Speed	Transfer function	MSE error
1	20	$\frac{2.557e-4}{s+3.102e-4}$	0.3202
	40	$\frac{2.454e-4}{s+5.232e-4}$	0.2475
	60	$\frac{1.781e-4}{s+5.156e-4}$	0.6504
	80	$\frac{1.396e-4}{s+6.072e-4}$	0.3042
	100	$\frac{8.05e-5}{s+5.412e-4}$	0.1794

Table 5. 2-pole transfer function model

Pole no.	Speed	Transfer function	MSE error
2	20	$\frac{-6.06e-8}{s^2+1.757e-3\,s+3.557e-14}$	113.9
	40	$\frac{4.607e-7}{s^2+1.908e-2\,s+1.377e-10}$	24.23
	60	$\frac{3.215e-7}{s^2+1.806e-2\,s+7.993e-11}$	30.16
	80	$\frac{3.487e-7}{s^2+2.883e-2\,s+8.761e-8}$	26.96
	100	$\frac{2.001e-7}{s^2+2.521e-2\,s+2.512e-9}$	17.91

Table 6. 3-pole transfer function model

Pole no.	Speed	Transfer Function	MSE error
3	20	$\frac{2.671e-9}{s^3+4.09e-3\,s^2+1.184e-5\,s+3.223e-9}$	0.2366
	40	$\frac{4.188e-9}{s^3+4.751e-3\,s^2+1.919e-5\,s+8.929e-9}$	0.1458
	60	$\frac{7.463e-9}{s^3+8.589e-3\,s^2+4.725e-5\,s+2.154e-8}$	0.4134
	80	$\frac{1.862e-9}{s^3+8.062e-3\,s^2+1.86e-5\,s+8.066e-9}$	0.2525
	100	$\frac{6.679e-10}{s^3+6707e-3\,s^2+1.198e-5\,s+4.473e-9}$	0.1533

Table 7. 4-pole transfer function model

Pole no.	Speed	Transfer function	MSE error
4	20	$\frac{-1.997e-13}{s^4+1.975e-3\,s^3+7.221e-6\,s^2+9.242e-9\,s+2.108e-22}$	89.82
	40	$\frac{1.412e-12}{s^4+1.125e-2\,s^3+3.639e-5\,s^2+4.029e-8\,s+2.204e-12}$	4.942
	60	$\frac{5.26e-13}{s^4+7.546e-3\,s^3+1.794e-5\,s^2+1.816e-8\,s+1.169e-12}$	6.995
	80	$\frac{4.613e-13}{s^4+6.91e-3\,s^3+1.931e-5\,s^2+1.752e-8\,s+1.778e-12}$	1.67
	100	$\frac{9.125e-14}{s^4+3.578e-3\,s^3+4.885e-6\,s^2+1.353e-8\,s+7.936e-21}$	18.17

3.2. System linearity analysis

Figure 5 from section 3.2 previously illustrates the plot of the pole location on the s-plane for the brush (representing a 3rd-order model). In both cases. The order of magnitude of the values of the poles is in the order of 10^{-3}. From the analysis of other components, a similar order of magnitude of the poles was also observed. This may allow an assumption that the poles are so close to each other that they are the same, and the system is LTI. To quantitatively evaluate the spread of the poles' values, the variance and coefficients of variation CV for all components at all speeds are computed and reported in Tables 8 and 9.

Table 8. Pole position, average, and variance for the component brush

Parameter		$\sigma_{Brush\ 1}$	$\sigma_{Brush\ 2}$	$\sigma_{Brush\ 3}$
Speed	20	$-1.89e-3+2.67e-3i$	$-1.89e-3-2.67e-3i$	$-3.0e-4$
	40	$-2.11e-3+3.54e-3i$	$-2.11e-3-3.54e-3i$	$-5.26e-4$
	60	$-4.05e-3+5.18e-3i$	$-4.05e-3-5.18e-3i$	$-4.98e-4$
	80	$-3.75e-3+5.73e-3i$	$-3.75e-3-5.73e-3i$	$-5.6e-4$
	100	$-3.98e-3$	$-2.22e-3$	$-5.06e-4$
$\overline{\sigma_k}$		$-3.2e-3+2.4e-3i$	$-2.8e-3-2.4e-3i$	$-4.78e-4$
S^2		$5.68e-6$	$5.57e-6$	$1.04e-8$
CV		0.74	0.84	0.22

Table 9. Pole position, average, and variance for the component bearing, permanent magnet, and casing

Parameter		$\sigma_{Bearing}$	$\sigma_{Perm.Magnet}$	σ_{Casing}
Speed	20	$-3.31e-4$	–3.4e–4	$-3.42e-4$
	40	$-5.09e-4$	–5.08e–4	$-5.10e-4$
	60	$-4.99e-4$	–4.94e–4	$-4.95e-4$
	80	$-5.84e-4$	–5.82e–4	$-5.87e-4$
	100	$-5.28e-4$	–5.22e–4	$-5.27e-4$
$\overline{\sigma_k}$		$-4.90e-4$	–4.89e–4	$-4.92e-4$
S^2		$8.97e-9$	8.05e–9	$8.31e-9$
CV		0.19	0.18	0.19

From Tables 8 and 9, the small values of variance should not be mistaken for a small spread. The CV value for the brush component is especially high where a maximum value of 0.84. In percentage, it is translated to 82%, which means the standard deviation is at 82% equal to the mean. This level of variability is significant because it means that the data points are spread out over a wide range relative to the mean. Other CVs for other components were also recorded at close to 0.2 or close to 20%, which signifies a relatively high variability. From the pole variances observation for data from different speeds, it can be assumed that the thermal system of the DC machine is not linear, thus non-LTI.

4. DISCUSSION

4.1. Identified transfer functions

The model estimation process indicated that a third-order transfer function provided the best fit for the brush component, with minimal MSE across all speeds. In contrast, the casing, bearing, and permanent magnet were adequately modeled using first-order transfer functions. This variation in model complexity suggests that different motor components exhibit distinct thermal behaviors, likely influenced by their physical structure and proximity to heat-generating sources.

The choice of transfer function order also highlights an important balance between model accuracy and stability. While higher-order models could capture the thermal dynamics accurately, they risk overfitting, as seen in initial trials with fourth-order models, which resulted in higher MSE. The observed stability of first- and third-order models demonstrates the suitability of these orders for practical applications. This could produce reliable yet computationally efficient thermal modeling. While this study focuses on models up to fourth order, future work could explore techniques like cross-validation and regularization to evaluate higher-order models while mitigating overfitting.

4.2. Coefficient of variation (CV) analysis

The coefficient of variation (CV) was computed for the poles of the identified transfer functions to assess the variability of thermal response across different speeds. Especially for the brush, the component exhibited the highest CV, with values reaching 0.84, indicating significant deviations from a linear behavior. This high variability suggests that the thermal response of the brush is highly sensitive to changes in speed, likely due to its direct interaction with the commutator, where frictional heat generation is non-linear. The modeling through a transfer function oversimplifies the thermal system and is unfit to represent the temperature response of the brush. In contrast, the casing and bearing showed much lower CV values (0.18-0.19), reflecting more stable thermal dynamics and a closer alignment with linear assumptions.

The disparity in CV values among components reinforces the need for variable or adaptive modeling approaches. While first-order transfer functions suffice for components with low CV, the brush's high variability suggests that linear models may inadequately capture its thermal behavior. This necessitates further exploration of non-linear thermal models, such as higher-order transfer functions or thermal networks, to improve accuracy for components with complex dynamics.

4.3. Limitations of the linear model

This finding of high variability implicates the limitation of linear models. They are unable to fully capture the complex and non-linear dynamics of heat generation and dissipation in certain motor components. For example, the brush, which interacts directly with the commutator, experiences frictional heat generation that is inherently non-linear, particularly under varying speeds and operating conditions. This is made more obvious and highlighted at the no-load condition, where the copper losses generated heat is at a minimum. To address these limitations, future research should explore nonlinear thermal models capable of capturing the complex dynamics of heat transfer. One obvious potential approach, continuing the spirit of using a transfer function, is by developing a nonlinear or adaptive transfer function. A new adaptive transfer

function that changes its pole values as a function of speed may better replicate the dynamic behavior. However, a lot more sampling of the temperature response at different speeds is first needed to make sure the model is accurate. Then, a function that relates the speeds and the pole values should be identified, before the function can be used to provide the variable pole value to the adaptive transfer function. Other solutions, especially the lumped parameter thermal network, were used in the literature with losses or thermal parameters being variable and modified using the feedback of speed. However, the nature of the model, having multiple nodes and multiple input losses calculation, makes it more complex to develop and requires slightly more computational resources.

Another limitation is related to the steady-state focused study. While this study focused on steady-state conditions under no-load operation, the findings lay the groundwork for further exploration of motor thermal behavior in dynamic environments. Specifically, future research will replicate the methodology for transient phases, such as start-up or acceleration, to develop a comprehensive transfer function thermal model that accounts for time-varying thermal responses. Additionally, studies incorporating loaded conditions could provide valuable insights into the interaction between speed- and load-dependent temperature increases, further enhancing the applicability of thermal models in real-world motor health monitoring systems.

5. CONCLUSION

In this study, the linearity of the thermal system of a brushed dc machine is studied using the transfer function across varying speeds. The results demonstrate that the thermal response of motor components varies significantly, with CV values ranging from 0.18 for the casing to 0.84 for the brush. These findings show significant deviations from linearity, particularly for the brush component, indicating that the system is non-linear and a single linear transfer function may not adequately model the thermal system.

The key contributions of this research include the development of a systematic framework for assessing thermal response variability using transfer functions and CV analysis. The demonstrated variability in thermal response suggests that monitoring solutions must account for non-linear behavior in critical components to improve fault detection accuracy. It also highlights the potential of transfer functions as a computationally efficient tool for thermal modeling in resource-constrained applications.

ACKNOWLEDGEMENTS

The authors would like to acknowledge the financial support by Universiti Malaysia Pahang Al-Sultan Abdullah under the Fundamental Research Grant No. PDU233210 and the Postgraduate Research Grant Scheme PGRS230324.

FUNDING INFORMATION

The study was funded by Universiti Malaysia Pahang Al-Sultan Abdullah under the Fundamental Research Grant No. PDU233210 and the Postgraduate Research Grant Scheme PGRS230324.

AUTHOR CONTRIBUTIONS STATEMENT

This journal uses the Contributor Roles Taxonomy (CRediT) to recognize individual author contributions, reduce authorship disputes, and facilitate collaboration.

Name of Author	C	M	So	Va	Fo	I	R	D	O	E	Vi	Su	P	Fu
M. S. Mat Jahak	✓	✓	✓	✓	✓	✓		✓	✓	✓			✓	
M. A. H. Rasid		✓				✓		✓	✓	✓	✓	✓		

C : **C**onceptualization
M : **M**ethodology
So : **So**ftware
Va : **Va**lidation
Fo : **Fo**rmal analysis
I : **I**nvestigation
R : **R**esources
D : **D**ata Curation
O : Writing - **O**riginal Draft
E : Writing - Review & **E**diting
Vi : **Vi**sualization
Su : **Su**pervision
P : **P**roject administration
Fu : **Fu**nding acquisition

CONFLICT OF INTEREST STATEMENT

Authors state no conflict of interest.

DATA AVAILABILITY

The data that support the findings of this study are available from the corresponding author, [MAHR], upon reasonable request.

REFERENCES

[1] IEA, "Energy-efficiency policy opportunities for electric motor-driven systems," Paris, 2011. [Online]. Available: https://www.iea.org/reports/energy-efficiency-policy-opportunities-for-electric-motor-driven-systems

[2] K. Sawa, T. Ueno, and H. Tanaka, "A study on wear of brush and carbon flat commutator of dc motor for automotive fuel pump," *IEICE Transactions on Electronics*, vol. E93-C, no. 9, pp. 1443–1448, 2010, doi: 10.1587/transele.E93.C.1443.

[3] J. J. R. Nicholas, "Off-line and on-line motor electrical monitoring and condition analysis: payoffs and problems," 1996.

[4] B. Wang, C. Lin, H. Inoue, and M. Kanemaru, "Induction motor eccentricity fault detection and quantification using topological data analysis," *IEEE Access*, vol. 12, pp. 37891–37902, 2024, doi: 10.1109/ACCESS.2024.3376249.

[5] D. Basak, A. Tiwari, and S. P. Das, "Fault diagnosis and condition monitoring of electrical machines - a review," in 2006 IEEE International Conference on Industrial Technology, IEEE, 2006, pp. 3061–3066. doi: 10.1109/ICIT.2006.372719.

[6] S. Nandi, H. A. Toliyat, and X. Li, "Condition monitoring and fault diagnosis of electrical motors - a review," in *IEEE Transactions on Energy Conversion*, 2005, pp. 719–729. doi: 10.1109/TEC.2005.847955.

[7] IEEE, "IEEE recommended practice for the design of reliable industrial and commercial power systems." IEEE, Piscataway, NJ, USA, Feb. 12, 2007. doi: 10.1109/IEEESTD.2007.380668.

[8] K. K. C. Deekshit, M. V. G. Rao, and R. S. Rao, "Fault indexing parameter based fault detection in induction motor via MCSA with wiener filtering," *Electric Power Components and Systems*, vol. 48, no. 19–20, pp. 2048–2062, 2021, doi: 10.1080/15325008.2021.1910376.

[9] D. Liu, H. Inoue, and M. Kanemaru, "Robust motor current signature analysis (MCSA)-based fault detection under varying operating conditions," in *2022 International Conference on Electrical Machines and Systems, ICEMS 2022*, 2022. doi: 10.1109/ICEMS56177.2022.9983454.

[10] K. C. D. Kompella, N. S. Rongala, S. R. Rayapudi, and V. G. R. Mannam, "Robustification of fault detection algorithm in a three-phase induction motor using mcsa for various single and multiple faults," *IET Electric Power Applications*, vol. 15, no. 5, pp. 593–615, 2021, doi: 10.1049/elp2.12049.

[11] E. Awada, A. Al-Qaisi, E. Radwan, and M. Nour, "Motor fault detection using sound signature and wavelet transform," *International Journal of Power Electronics and Drive Systems*, vol. 13, no. 1, pp. 247–255, 2022, doi: 10.11591/ijpeds.v13.i1.pp247-255.

[12] J. W. Hur and T. A. Shifat, "Motor vibration analysis for the fault diagnosis in non-stationary operating conditions," *International Journal of Integrated Engineering*, vol. 12, no. 3, pp. 151–160, 2020, doi: 10.30880/ijie.2020.12.03.019.

[13] M. S. Rafaq *et al.*, "A simple method for identifying mass unbalance using vibration measurement in permanent magnet synchronous motors," *IEEE Transactions on Industrial Electronics*, vol. 69, no. 6, pp. 6441–6444, 2022, doi: 10.1109/TIE.2021.3088332.

[14] M. R. Barusu and M. Deivasigamani, "Non-invasive vibration measurement for diagnosis of bearing faults in 3-phase squirrel cage induction motor using microwave sensor," *IEEE Sensors Journal*, vol. 21, no. 2, pp. 1026–1039, 2021, doi: 10.1109/JSEN.2020.3004515.

[15] S. Lu, G. Qian, Q. He, F. Liu, Y. Liu, and Q. Wang, "In situ motor fault diagnosis using enhanced convolutional neural network in an embedded system," *IEEE Sensors Journal*, vol. 20, no. 15, pp. 8287–8296, Aug. 2020, doi: 10.1109/JSEN.2019.2911299.

[16] Y. Zhou, Q. Shang, and C. Guan, "Three-phase asynchronous motor fault diagnosis using attention mechanism and hybrid CNN-MLP by multi-sensor information," *IEEE Access*, vol. 11, pp. 98402–98414, 2023, doi: 10.1109/ACCESS.2023.3307770.

[17] K. Yatsugi, S. E. Pandarakone, Y. Mizuno, and H. Nakamura, "Common diagnosis approach to three-class induction motor faults using stator current feature and support vector machine," *IEEE Access*, vol. 11, pp. 24945–24952, 2023, doi: 10.1109/ACCESS.2023.3254914.

[18] M. A. H. Rasid, M. N. A. Zulkafli, and D. M. Nafiz, "Evaluation of dc machine armature winding temperature estimation using temperature measured on brush and bearing," in *2022 IEEE 1st Industrial Electronics Society Annual On-Line Conference (ONCON)*, IEEE, Dec. 2022, pp. 1–6. doi: 10.1109/ONCON56984.2022.10126816.

[19] P. Gangsar and R. Tiwari, "Signal based condition monitoring techniques for fault detection and diagnosis of induction motors: a state-of-the-art review," *Mechanical Systems and Signal Processing*, vol. 144, p. 106908, Oct. 2020, doi: 10.1016/j.ymssp.2020.106908.

[20] H. Wu and I. Dobson, "Cascading stall of many induction motors in a simple system," *IEEE Transactions on Power Systems*, vol. 27, no. 4, pp. 2116–2126, Nov. 2012, doi: 10.1109/TPWRS.2012.2189420.

[21] M. Syawal, M. Jahak, M. Azri, H. Rasid, I. Ishak, and S. Puteh, "Thermal monitoring and modelling of eletrical machine – a review," *Mekatronika: Journal of Intelligent Manufacturing and Mechatronics*, vol. 6, no. 1, pp. 1–6, 2024, doi: 10.15282/mekatronika.v6i1.9898.

[22] R. Sundararajan, V. Natarajan, V. Viswanathan, and S. H. R. Shankar, "Automatic temperature control of electric motor using PIC microcontroller," *2022 IEEE Delhi Section Conference, DELCON 2022*, 2022, doi: 10.1109/DELCON54057.2022.9752892.

[23] G. Guo and W. Cai, "Prediction of electromagnetic vibration with simulated transfer function for interior permanent magnet synchronous motor," *IEEE Transactions on Energy Conversion*, vol. 38, no. 4, pp. 2584–2595, Dec. 2023, doi: 10.1109/TEC.2023.3292061.

[24] H. Miloudi, A. Bendaoud, M. Miloudi, S. Dickmann, and S. Schenke, "A novel method of transfer-function identification for modeling dm impedance of ac motor," in *2017 International Symposium on Electromagnetic Compatibility - EMC EUROPE*, IEEE, Sep. 2017, pp. 1–5. doi: 10.1109/EMCEurope.2017.8094770.

[25] M. Straka, M. Mares, and O. Horejs, "The impact of key temperature measuring points on thermal error compensation model transfer between milling centers of the same product line," *MM Science Journal*, vol. 2021-November, pp. 5211–5218, 2021, doi: 10.17973/MMSJ.2021_11_2021173.

[26] H. Zhang, "Online thermal monitoring models for induction machines," *IEEE Transactions on Energy Conversion*, vol. 30, no. 4, pp. 1279–1287, Dec. 2015, doi: 10.1109/TEC.2015.2431444.

[27] P. Zhang, Y. Du, and T. G. Habetler, "A transfer-function-based thermal model reduction study for induction machine thermal overload protective relays," *IEEE Transactions on Industry Applications*, vol. 46, no. 5, pp. 1919–1926, Sep. 2010, doi: 10.1109/TIA.2010.2058831.
[28] N. Fatimah Abdullah, A. A. Wahab, and M. A. H. Rasid, "Study of temperature rise of small brushed DC motor under different load," *MATEC Web of Conferences*, vol. 225, p. 03010, Nov. 2018, doi: 10.1051/matecconf/201822503010.
[29] R. Choupanzadeh and A. Zadehgol, "Stability, causality, and passivity analysis of canonical equivalent circuits of improper rational transfer functions with real poles and residues," *IEEE Access*, vol. 8, pp. 125149–125162, 2020, doi: 10.1109/ACCESS.2020.3007854.
[30] F. Golnaraghi and B. C. Kuo, "Automatic control systems(10th Edition)," In McGraw-Hill Education, 2017.
[31] F. S. M. Al Khafaji, W. Z. Wan Hasan, M. M. Isa, and N. Sulaiman, "A hsmdaq system for estimating transfer function of a DC motor," in *2019 IEEE Asia Pacific Conference on Postgraduate Research in Microelectronics and Electronics (PrimeAsia)*, IEEE, Nov. 2019, pp. 25–28. doi: 10.1109/PrimeAsia47521.2019.8950719.
[32] Y. Naung, A. Schagin, H. L. Oo, K. Z. Ye, and Z. M. Khaing, "Implementation of data driven control system of dc motor by using system identification process," in *2018 IEEE Conference of Russian Young Researchers in Electrical and Electronic Engineering (EIConRus)*, IEEE, Jan. 2018, pp. 1801–1804. doi: 10.1109/EIConRus.2018.8317455.
[33] T. Sadeq and C. K. Wai, "Model the DC-DC converter with supercapacitor module based on system identification," *2019 IEEE International Conference on Automatic Control and Intelligent Systems, I2CACIS 2019 - Proceedings*, pp. 185–188, 2019, doi: 10.1109/I2CACIS.2019.8825095.

BIOGRAPHIES OF AUTHORS

M. S. Mat Jahak received his bachelor degree in mechatronics engineering from the Faculty of Manufacturing and Mechatronics Engineering Technology, UMPSA. He is currently working towards his master's degree. He has experience in assisting the faculty in teaching various subjects including microcontrollers, digital electronics, analog electronics, and automated manufacturing systems. He can be contacted at email: muhdsyawalmatjahak@gmail.com.

M. A. H. Rasid received his Ph.D. degree in mechatronics from Université de Technologie de Compiègne, France in 2016. He is also an IEEE Senior member. He is currently a senior lecturer in the Faculty of Manufacturing and Mechatronics Engineering Technology, Universiti Malaysia Pahang. He is a researcher belonging to the Mechatronics Systems and Design Research Group. His research focuses on electromechanical systems with a multiphysics approach, focusing on thermal and vibroacoustic behavior. His teaching areas include electrical engineering, mechatronics, and controls. He can be contacted at email: mahizami@umpsa.edu.my.